ORIGINAL RESEARCH

Metabolic Adaptation in Methicillin-Resistant *Staphylococcus aureus* Pneumonia

Stanislaw J. Gabryszewski[1]*, Tania Wong Fok Lung[1]*, Medini K. Annavajhala[2,3], Kira L. Tomlinson[1], Sebastian A. Riquelme[1], Ibrahim N. Khan[1], Loreani P. Noguera[1], Matthew Wickersham[1], Alison Zhao[1], Arielle M. Mulenos[4], David Peaper[5], Jonathan L. Koff[4], Anne-Catrin Uhlemann[2,3], and Alice Prince[1]

[1]Department of Pediatrics, [2]Department of Medicine, and [3]Microbiome and Pathogen Genomics Core, Department of Medicine, Columbia University Irving Medical Center, New York, New York; and [4]Department of Internal Medicine and [5]Department of Laboratory Medicine, Yale University School of Medicine, New Haven, Connecticut

ORCID ID: 0000-0002-7399-9295 (A.P.).

Abstract

Methicillin-resistant *Staphylococcus aureus* (MRSA) is a versatile human pathogen that is associated with diverse types of infections ranging from benign colonization to sepsis. We postulated that MRSA must undergo specific genotypic and phenotypic changes to cause chronic pulmonary disease. We investigated how MRSA adapts to the human airway to establish chronic infection, as occurs during cystic fibrosis (CF). MRSA isolates from patients with CF that were collected over a 4-year period were analyzed by whole-genome sequencing, transcriptional analysis, and metabolic studies. Persistent MRSA infection was associated with staphylococcal metabolic adaptation, but not changes in immunogenicity. Adaptation was characterized by selective use of the tricarboxylic acid cycle cycle and generation of biofilm, a means of limiting oxidant stress. Increased transcription of specific metabolic genes was conserved in all host-adapted strains, most notably a 10,000-fold increase in *fumC*, which catalyzes the interconversion of fumarate and malate. Elevated fumarate levels promoted *in vitro* biofilm production in clinical isolates. Host-adapted strains preferred to assimilate glucose polymers and pyruvate, which can be metabolized to generate N-acetylglucosamine polymers that comprise biofilm. MRSA undergoes substantial metabolic adaptation to the human airway to cause chronic pulmonary infection, and selected metabolites may be useful therapeutically to inhibit infection.

Keywords: bacterial metabolic adaptation; chronic pulmonary infection; *Staphylococcus aureus*; cystic fibrosis

Clinical Relevance

This study should be of substantial interest to the cystic fibrosis community, as well as to critical care, pulmonary, and infectious disease physicians who deal with the treatment of *Staphylococcus aureus* pneumonia. Our findings indicate that "host-adapted" *S. aureus* strains retain their immunogenicity and do not necessarily become less virulent over time. In addition, these findings lend support to the concept of targeting bacterial metabolism as a mechanism to prevent bacterial metabolic reprogramming, biofilm formation, and the development of chronic airway infection.

Staphylococcus aureus is a frequent cause of pulmonary infection targeting individuals with underlying pulmonary conditions, including intubation, chronic obstructive pulmonary disease (COPD), and especially cystic fibrosis (CF). *S. aureus* pulmonary infections, particularly those caused by methicillin-resistant *S. aureus* (MRSA), are refractory to antibiotic treatment and often portend a poor prognosis (1–3). Exactly how *S. aureus* transitions from a nasal commensal to a pulmonary pathogen

(Received in original form November 27, 2018; accepted in final form February 11, 2019)

*These authors contributed equally to this work.

Supported by Cystic Fibrosis Foundation (CFF) grant CFF Prince 18G0 and National Institutes of Health (NIH) grants R35HL135800 and S10RR027050.

Author Contributions: S.J.G., T.W.F.L., A.-C.U., and A.P. designed experiments. S.J.G., T.W.F.L., M.K.A., K.L.T., S.A.R., I.N.K., L.P.N., M.W., A.Z., and A.-C.U. performed experiments and analyzed data. A.M.M., D.P., and J.L.K. generated and analyzed data. S.J.G., T.W.F.L., and A.P. wrote the manuscript.

Correspondence and requests for reprints should be addressed to Alice Prince, M.D., Department of Pediatrics, Columbia University, Black Building, Room 4-416, 650 W. 168th Street, New York, NY 10032. E-mail: asp7@columbia.edu.

Am J Respir Cell Mol Biol Vol 61, Iss 2, pp 185–197, Aug 2019

Originally Published in Press as DOI: 10.1165/rcmb.2018-0389OC on February 11, 2019
Internet address: www.atsjournals.org

remains unclear. Moreover, the impact of adaptive changes to the human airway on the virulence of these organisms is poorly understood.

Both the host and infecting bacteria undergo metabolic adjustments to cope with the demands of infection. Immune cells (e.g., macrophages) switch from oxidative phosphorylation to aerobic glycolysis (4) to generate ATP while regulating the release of reactive oxygen species and immunoreactive metabolites. Concurrently, bacteria adjust their metabolic activity to fuel the production of surface and secreted proteins required to thwart immune clearance mechanisms, including reactive oxygen species, while also limiting the generation of endogenous oxidants. Bacterial metabolic reprogramming (5) is a widely conserved mechanism by which bacteria preferentially use metabolic pathways to generate antioxidant NADPH while supporting gluconeogenesis to provide substrates for extracellular polysaccharides, which are important for biofilm formation (6). Although staphylococcal biofilm production has been best characterized in the setting of skin/soft tissue- and catheter-associated infections (7), it is likely that biofilms also play an important role in the setting of lung infection.

The prolonged course of bacterial colonization and infection in CF allows for a longitudinal study of the commensal-to-pathogen transition of *S. aureus*. Murine studies have identified specific toxins, especially α-toxin, as critical for the establishment of an acute infection (8). However, identification of the bacterial determinants of chronic infection has been challenging. Epidemiological studies have not revealed major genomic differences between nasal colonizers and organisms that cause severe infections (9). Transcriptomic studies of CF-associated *S. aureus* have implicated genes involved in immune evasion, toxin production, iron scavenging, and intercellular adhesion (10, 11) in adaptation to the host.

In this work, we used sequential isolates of MRSA obtained from chronically infected adult patients with CF to study how clinical isolates of *S. aureus* adapt to the airway, as compared with the standard laboratory strain LAC USA300 MRSA. Using genomic, metabolic, and gene expression studies, we demonstrate that host-adapted MRSA undergoes substantial metabolic reprogramming, allowing for the use of available carbon sources to simultaneously promote biofilm production and limit oxidant generation.

Some of the results of these studies have been previously reported in the form of an abstract (12).

Methods

Bacterial Isolation from Patients

MRSA isolates were obtained from the sputum, blood, or BAL fluid (BALF) of three patients with CF who were being cared for at a CF center as part of routine care and ongoing epidemiological surveillance. The *fumC* transposon mutant from the NTML transposon library was in the JE2 background (13).

Bacterial Culture

Bacteria were cultured at 37°C in Luria-Bertani broth, with shaking at 250 rpm. Overnight cultures were subinoculated at 1:100 and grown to an OD_{600} of 1. Growth curves were performed in 96-well plates inoculated with a 1:100 dilution of overnight cultures and monitored using a BioTek Synergy H1 microplate reader with Gen5 software. Bacterial growth was similarly determined in the presence or absence of 1.2 mM paraquat (Sigma-Aldrich) or select carbon sources (5–500 mM sodium acetate, sodium citrate, disodium succinate; Sigma-Aldrich).

Whole-Genome Sequencing and Hybrid Assembly

Genomic DNA was extracted using a Qiagen DNeasy UltraClean Microbial DNA Isolation Kit. A Nextera XT DNA Library Prep Kit was used to prepare barcoded libraries, which were sequenced using an Illumina MiSeq v3 sequencing kit. Multilocus sequence typing and characterization of antibiotic-resistance genes was performed using SRST2 (14). To generate accurate reference genomes for isolate series, we also conducted long-read sequencing of strains A1, B1, and C1 on a MinION (Oxford Nanopore Technologies) after library preparation with the Rapid Barcoding Sequencing Kit. Reads were basecalled using MinKnow and Epi2ME (Metrichor), and hybrid *de novo* assembly of Nanopore and Illumina reads was performed using SPAdes v3.10.1 (6). The genome was annotated using Prokka v1.12 (15), and mobile genetic elements and prophage regions were identified by IslandViewer 4 (16) and PHASTER (17), respectively. We used Snippy software (Snippy v3, https://github.com/tseemann/snippy) to identify core genome concatenated SNPs.

Phylogenetic Analysis

We constructed phylogenetic trees by mapping individual reads from each isolate against the curated *S. aureus* sequence type 105 (ST105) genome using Snippy v3 after excluding mobile genetic elements and prophage regions. Maximum-likelihood phylogenetic analysis based on core genome concatenated SNPs was performed using RAxML v8.0.0 with 100 bootstrap inferences and the GTR GAMMA model. Phylogenetic trees were visualized using iTOL v3 (18).

RNA Isolation and qRT-PCR

For bacterial RNA isolation, bacteria were grown statically for 24 hours in tryptic soy broth (TSB) containing 0.5% glucose. The bacteria were harvested by centrifugation, stored in RNAProtect (QIAGEN), and normalized based on OD_{600}. Bacterial pellets were incubated in lysis buffer (50 μM Tris-EDTA [pH 7.5], 8 U/ml mutanolysin [Sigma], 0.018 mg/ml lysostaphin [Sigma], 0.05 g/ml lysozyme [Sigma]) at 37°C for 45 minutes, and TRK lysis buffer (Omega Bio-tek) was added. After 10 minutes at room temperature, 70% ethanol was added and the samples were transferred to EZNA RNA isolation kit columns (Omega Bio-tek). RNA was isolated according to the manufacturer's instructions and treated with a DNA-free DNase treatment and removal kit (Invitrogen). RNA quality was verified using a NanoDrop spectrophotometer (NanoDrop Technologies). A SuperScript III RT kit (Invitrogen) was used to generate cDNA for qRT-PCR reactions with SYBR green reagents (Applied Biosystems). qRT-PCR was performed using a StepOne Plus thermal cycler (Applied Biosystems), and data were analyzed using the ΔΔCt method. The qRT-PCR primers are listed in Table 1. Primers directed against the 16S rRNA

Table 1. List of Primers Used in this Study

Primers Used for qRT-PCR			
Target Gene	**Gene**	**Forward Primer Sequence**	**Reverse Primer Sequence**
Citrate synthase	*gltA*	5′-gatctagctgaaaacgcgca-3′	5′-ctgtcattggatgcacgtga-3′
Aconitase	*acnA*	5′-gcaaacatggcaccagagta-3′	5′-tttggtcctgaaagcgatgc-3′
Isocitrate dehydrogenase	*icd/citC*	5′-ccagctgagcatgatgttgt-3′	5′-ggagctgtaccatgtgttgc-3′
2-oxoglutarate dehydrogenase	*sucA*	5′-gccgtgttacatgatgagca-3′	5′-caccatattgcgcttcccaa-3′
2-oxoglutarate dehydrogenase	*sucB*	5′-tgctatcatcggcgaaggta-3′	5′-tgacaccattttcacgagca-3′
Succinyl coA synthetase	*sucC*	5′-tagaggtaaagcaggcggag-3′	5′-cccttcttcagacgccatca-3′
Succinyl coA synthetase	*sucD*	5′-caccatttgctgcagactca-3′	5′-atcacacctggacagttcgg-3′
Succinate dehydrogenase	*sdhA*	5′-tgtatggtggcgacttcctt-3′	5′-ttgttgtccagttgttgccc-3′
Succinate dehydrogenase	*sdhB*	5′-ggaccacgtatgccagagaa-3′	5′-ctgtaagccaccagtaccca-3′
Fumarase	*fumC*	5′-atgcttgaccgttgcgaaat-3′	5′-agcgccttcaatgttccatg-3′
Malate:quinone oxidoreductase	*mqo1*	5′-atgctatcgtgatgaattcaaagg-3′	5′-ttatttaacttgtaaatacttagttac-3′
Glucose-6-phosphate 1-dehydrogenase	*zwf*	5′-caaacacatcccatgtttaatcaca-3′	5′-tggaatattgatggaaacaacttacg-3′
Glyceraldehyde 3-phosphate dehydrogenase	*gapA*	5′-attgaagcaggcgctaaaaa-3′	5′-ctgtgaggtgcgtcttgtgt-3′
Glycolytic operon regulator	*gapR*	5′-ttgcaagcacagcaaaagc-3′	5′-ccatatgttcgcttaaacttcg-3′
c-di-AMP synthase	*dacA*	5′-tgcggttggtatttcagaag-3′	5′-tttcttttgaaagcgtgtgc-3′
c-di-AMP phosphodiesterase	*gdpP*	5′-ttagtcgatgggcaactgag-3′	5′-ttaattgggcacgataacca-3′
Intercellular adhesion A	*icaA*	5′-acacttgctggcgcagtcaa-3′	5′-tctggaaccaacatccaaca-3′
Intercellular adhesion B	*icaB*	5′-tccttatggcttgatgaatgacg-3′	5′-ctaatctttttcatggaatccgtcc-3′
Intercellular adhesion C	*icaC*	5′-atgggttataactacgaacgtg-3′	5′-cgtgcaaatacccaagataac-3′
Intercellular adhesion D	*icaD*	5′-atggtcaagcccagacagag-3′	5′-agtattttcaatgtttaaagcaa-3′
Lipoteichoic acid synthase	*ltaS*	5′-attctcatttaattacattgactaacc-3′	5′-ccatcaactgttgcatcacct-3′

gene were used as the housekeeping gene control. Additional controls included "no reverse transcriptase" and "no template" controls.

Biofilm Assays

Bacterial cultures were normalized to an OD_{600} of 1.0 and inoculated at 1:100 into TSB supplemented with 0.5% glucose in a 96-well plate. Sodium fumarate (Sigma-Aldrich) and L-malic acid (Sigma-Aldrich) were used at final concentrations of 62.5 mM, 125 mM, 250 mM, and 500 mM in TSB containing 0.5% glucose. Biofilm cultures were grown statically at 37°C. After 24 hours, OD_{600} was measured and plates were washed twice with water, dried, and fixed with methanol. They were then stained with 1% crystal violet (wt/vol) and again washed twice with water and dried. After solubilization of the well contents with 33% acetic acid (vol/vol), OD_{540} values were determined.

Extracellular DNA Quantification

Supernatants from the biofilm experiments were transferred to a new 96-well V-bottom plate and centrifuged (2,500 rpm, 5 min). The supernatants were then transferred to new wells and stained for 10 minutes with 1 μM (final concentration) SYTOX Blue stain (Invitrogen). Fluorescence was determined using a Tecan Infinite M200 plate reader, with excitation and emission spectra of 444 nm and 480 nm, respectively.

Congo Red Susceptibility Assays

Bacterial strains were grown in Luria-Bertani broth to an OD_{600} of 1 and serially diluted before they were plated on tryptic soy agar agar plates with or without 0.08% (wt/vol) Congo Red stain. The plates were incubated at 37°C overnight, and colonies were enumerated after 24 hours.

Carbon Source Use Assays

Carbon use was assessed via Biolog PM1 assays according to the manufacturer's instructions.

Cell Culture and Infections

Human bronchial epithelial (16HBE) cells were cultured in BronchiaLife medium (Lifeline Cell Technology) supplemented with 1% FBS and 1% penicillin/streptomycin. THP-1 cells were grown in RPMI 1640 medium (Corning) supplemented with 10% FBS and 1% penicillin/streptomycin. All cells were incubated at 37°C in 5% CO_2.

Gentamicin Protection Assays

THP-1 cells were infected at a multiplicity of infection of 10. For time points exceeding 30 minutes, the cells were washed 1 hour after infection and replaced with RPMI containing gentamicin at a final concentration of 0.5 mg/ml. The cells were washed with PBS at the desired time point, harvested by disassociating them with TrypLE Express cell dissociation enzyme (Life Technologies), serially diluted, and plated.

Mouse Infections and Sample Collection

Mouse care, anesthesia, and infections were performed in accordance with an institutionally approved protocol (AAAR9403). For infections, 6-week-old C57BL/6 mice were anesthetized with ketamine/xylazine and intranasally inoculated with 4×10^7 cfu (50 μl total volume) of *S. aureus* strains or PBS vehicle control. The mice were killed 24 hours after infection with pentobarbital, followed by collection of BALF and lungs. Lung cell homogenates were generated using 40 μm nylon cell strainers (Falcon). Bacteria in the BALF and lung cell homogenates were enumerated after serial dilution and plating on CHROMagar plates (BD).

Cytokine Analysis

After centrifugation to remove cellular content, samples were analyzed by multiplex cytokine array assays (Eve Technologies). IFN-β levels were assessed by ELISA (R&D) according to the manufacturer's instructions.

Flow Cytometric Analysis

BALF and lung cell suspensions were centrifuged (1,500 rpm, 6 min), and red blood cells were lysed with ammonium-chloride-potassium lysis buffer. Cells were resuspended in staining buffer and transferred to a V-bottom 96-well plate treated with DAPI and stained with a panel of antibodies (CD45-AF700, CD11b-

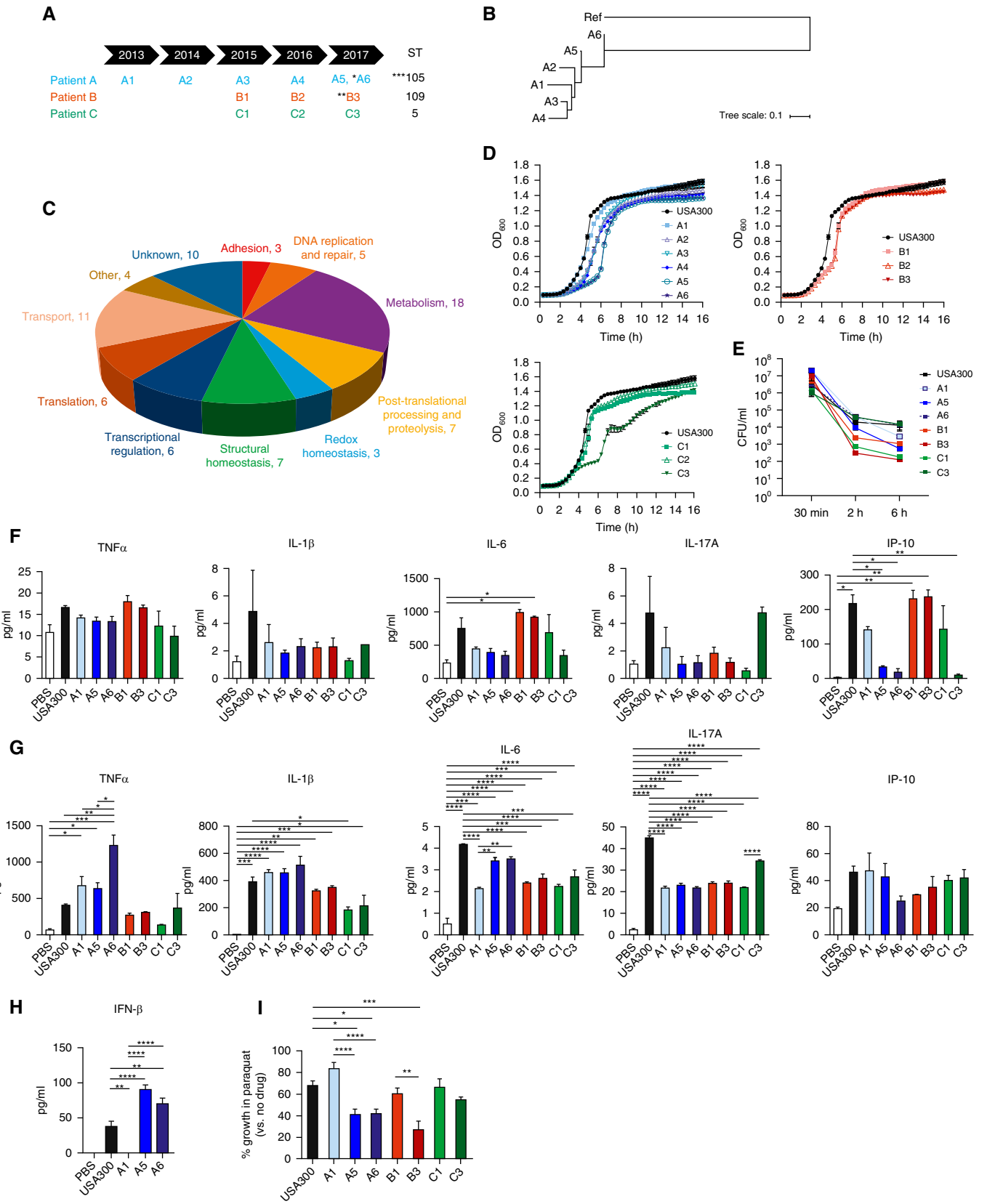

Figure 1. Characterization of cystic fibrosis (CF) host-adapted methicillin-resistant *Staphylococcus aureus* (MRSA) strains. (*A*) Timeline and sequence type (ST) of MRSA isolation from patients A, B, and C. All samples were harvested from sputum, with the exception of A6 (*, blood) and B3 (**, pleural fluid).

Table 2. Clinical Characteristics of the Patients from Whom MRSA Isolates were Collected

	Patients' Clinical Characteristics		
	Patient A	**Patient B**	**Patient C**
Age	45	27	41
Sex	Female	Male	Male
Sweat chloride values, mmol/L	97	87	34/36
CFTR genotype	ΔF508/ΔF508	R1162X/R347P	c.273+1G>A and c.3718-2477C>T with 7T/7T poly-T variants
FEV_1			
Most recent, L, % predicted	1.88 L (69%)	3.24 L (76%)	0.99 L (23%)
At admission, L, % predicted	1.37 L (51%)	2.93 L (70%)	0.87 L (20%)
CF-related complications	CF-related diabetes, pancreatic insufficiency	Pancreatic insufficiency	Pancreatic insufficiency
Acute presentation, 02/2017	Pneumonia with bacteremia	Pneumonia with right pleural effusion	Lobar pneumonia
Site of specimen collection	Sputum (A1–A5), blood (A6)	Sputum (B1–B2), BAL fluid (B3)	Sputum (C1–C3)
Period of MRSA collection	2013–2017 2013 (A1) 2014 (A2) 2015 (A3) 2016 (A4) 2017 (A5–A6)	2013–2017 2013 (B1) 2016 (B2) 2017 (B3)	2015–2017 2015 (C1) 2016 (C2) 2017 (C3)
Bacteriology, others (2017)	*Pseudomonas aeruginosa*	MSSA, *Haemophilus parainfluenzae*, *P. aeruginosa*	MSSA, *H. influenzae*, *Escherichia coli*

Definition of abbreviations: CF = cystic fibrosis; FEV_1 = forced expiratory volume in 1 second; MRSA = methicillin-resistant *Staphylococcus aureus*; MSSA = methicillin-sensitive *S. aureus*;

AF594, Ly6G-PercPCy5.5, Ly6C-BV421, CD11c-BV605, MHCII-APC-Cy7, SiglecF-APC/AF647, and Pro-IL1β-PeCy7). Cells were fixed in 10% paraformaldehyde solution and analyzed using a BD LSRII flow cytometer and FlowJo v10 software. Cell surface staining to identify cell types included alveolar macrophages ($CD45^+CD11b^{lo}$; $SiglecF^{hi}CD11c^+Ly6G^-Ly6C^-$), eosinophils ($CD45^+CD11b^{lo}$; $SiglecF^{lo}CD11c^-Ly6G^-Ly6C^-$), neutrophils ($CD45^+CD11b^{hi}SiglecF^{lo}$; $CD11c^-MHCII^-Ly6G^+Ly6C^{lo}$), and monocytes ($CD45^+CD11b^{hi}SiglecF^{lo}$; $CD11c^-MHCII^-Ly6G^-Ly6C^{lo/hi}$). For a given condition, the absolute numbers of recruited immune cells represent the product of the percentage of viable cells that exhibited a specific set of cell surface markers and the viable cell count, as determined using a Countess automated cell counter (Invitrogen).

Data Analysis and Statistics

Data were plotted with SE of mean, and statistical significances were determined using GraphPad Prism 7 software.

Results

Host-adapted MRSA Strains Acquire Mutations Predominantly in Genes Affecting Metabolism

MRSA isolates obtained from three patients with CF (patients A, B, and C) over a period of 2–4 years, with the most recent isolate taken at the time of an acute exacerbation, associated with bacteremia, lobar consolidation, or empyema, were studied by whole-genome sequencing (Figure 1A). The patients had distinct *Cftr* genotypes, with clinical severity ranging from a forced expiratory volume in 1 second (FEV_1) of 20% to 70% at the time of acute exacerbation, and had been coinfected with methicillin-sensitive *S. aureus* (MSSA), *Pseudomonas aeruginosa*, and *Haemophilus* species in the recent past (Table 2). We observed patient-specific clonality with distinct STs: ST105 (A), ST109 (B), and ST5 (C). To compare the evolution of SNPs among the patients' MRSA isolates, we *de novo* assembled the genomes of each initial isolate (A1, B1, and C1). The serial isolates from each patient differed by a substantial number of SNPs over the 2- to 4-year collection period. There are inherent difficulties in determining true insertion or

Figure 1. (Continued). A2–A6 were one-SNP variants of ST105 (***). (*B*) Phylogenetic tree of MRSA isolates from the A series, with an ST-matched non-CF isolate (CP011147) serving as a reference. Branch lengths represent the number of nucleotide substitutions per site. (*C*) Schematic diagram showing the number of nonsynonymous mutations (NSMs) observed among A-series MRSA isolates as compared with a non-CF reference strain, and their associated pathway. (*D*) Growth curves of the laboratory strain of MRSA USA300 and the isolates from the A, B, and C series in Luria-Bertani broth. Data shown are from four biological replicates in triplicate. (*E*) Intracellular bacterial persistence of the MRSA isolates from patients A, B, and C in THP-1 cells. Data shown are from two independent experiments with each sample in triplicate. (*F*) Cytokines from 16HBE cells infected with MRSA isolates. (*G*) Cytokines from THP-1 cells infected with MRSA isolates. (*H*) IFN-β production by 16HBE cells 24 hours after *S. aureus* infection. Data are shown for three independent experiments in triplicate. (*I*) Impact of the superoxide generator paraquat on growth of the MRSA isolates. Data shown are from two independent experiments in triplicate. Statistical significance was determined by one-way ANOVA, $^{****}P < 0.0001$, $^{***}P < 0.001$, $^{**}P < 0.01$, and $^{*}P < 0.05$. OD = optical density; Ref = reference non-CF isolate CP011147 strain.

deletion of bases (indels) from short read sequencing, as these often occur in regions of a gene with numerous repetitive sequences that could also arise due to mapping difficulties. For this reason, indels were not included in our analyses. The six isolates from patient A differed by 44 SNPs in total and 27 nonsynonymous mutations (NSMs), the three isolates from patient B differed by 24 SNPs in total and 17 NSMs, and the three isolates from patient C differed by 50 SNPs in total and 27 NSMs (Table 3 and Figure 1A). When compared with an ST-matched (ST105), non-CF reference strain (CP011147), the A-series isolates differed by 192 SNPs overall and 80 NSMs, 10 of which represented polymorphic sites among the A-series isolates themselves (Table 3 and Figure 1B). Based on pathway categorization, most of these mutations were in genes involved in metabolism and transport (Figure 1C). No mutations were observed in the virulence-associated *agr* locus, although mutations in *saeR*, which encodes part of a two-component regulatory system involved in virulence gene expression, were observed in the A series.

The accumulated mutations had minimal effects on growth rates (Figure 1D), as all strains achieved comparable densities by the stationary phase despite differences in lag and log phases in some isolates. Uptake and persistence within immune cells (THP-1, a human monocyte-macrophage cell line) were variable and, in most instances, comparable to those observed in the USA300 MRSA control (Figure 1E). Immunogenicity was assessed by quantifying cytokine expression induced in either human airway cells (16HBE) (Figure 1F) or THP-1 cells (Figure 1G). No global differences in immunogenicity were identified, but strain-dependent trends were observed. The later A-series isolates stimulated more IFN-β secretion in 16HBEs than the initial isolate (Figure 1H). The clinical strains appeared to become less resistant to oxidant stress over time, as assessed by susceptibility to the superoxide-generating agent paraquat (Figure 1I).

Host-adapted MRSA Strains Produce Biofilm

The A-series isolates developed mutations in *dacA* and *gpdP*, which encode a diadenylate cyclase required for the synthesis of cyclic-di-AMP (c-di-AMP) and a phosphodiesterase responsible for its hydrolysis, respectively (Figure 2A). c-di-AMP is a multifunctional bacterial secondary metabolite that controls the expression of many genes in response to environmental conditions, including those involved in biofilm formation. Increasing amounts of biofilm production was noted in later A and C isolates (Figure 2B). Transcriptional analysis of *dacA* and *gpdP* (Figure 2C) suggested a trend toward increased expression of both genes over time, roughly comparable to the biofilm phenotype (Figure 2B). As this was not a linear relationship, there are likely multifactorial means of regulation of c-di-AMP metabolism in the setting of CF host adaptation (Figure 2C). This highlights the contribution of both genetic and transcriptional changes in c-di-AMP metabolism to biofilm formation by host-adapted strains. In addition, the A6 isolate harbored an NSM mutation in the *saeR* locus, which is responsive to cellular metabolism and involved in biofilm formation (19).

Significant variability in colony size was noted among all clinical isolates examined in this study. Susceptibility to Congo Red (Figure 2D), an azo dye that directly targets and inhibits the activity of lipoteichoic acid synthase (LtaS) (20), was increased in the A series (A3, A5, and A6) as well as in isolate C3. These phenotypes correlated with increased expression of *ltaS*, a gene that is important for the biosynthesis of polyglycerolphosphate and is a critical component of the staphylococcal lipoteichoic acid cell wall (20, 21). These findings indicate alterations in cell wall structure, possibly reflecting adaptation to antimicrobial exposure. We also looked specifically at the expression of genes involved in *S. aureus* biofilm production, which can involve either the release of extracellular DNA (22) or the production of poly-N-acetyl-β-(1-6)-glucosamine. None of the strains shed extracellular DNA (Figure 2E), suggesting that biofilm formation was most likely due to expression of the intercellular adhesion locus (*icaA/B/C/D*) and production of poly-N-

Table 3. List of Nonsynonymous Mutations that Differed between at Least One of the A-Series Strains and a Sequence Type–matched, Non–Cystic Fibrosis Strain, or among Strains Harvested from a Single Patient

Isolate	Number of NSMs	Implicated Genes and Pathways
A vs. reference	80	Adhesion (*sdrC*, *fnbpb*) DNA replication and repair (*gyrA*, *addA*, *recN*) Metabolism (*adhE*, *sufS*, *trpG*, *ilvB*, *hisA*, *deoD*, *purI*, *rny*, *malX*, *araB*, *tktA*, *pckA*, *nagB*, *rpoB*, *mvaK2*, *malA*, *dagK*) Post-translational processing and proteolysis (*pepF*, *pepA2*, *pepX*, *aur*, *ureE*) Redox homeostasis (*hmp*, *ndhF*) Structural homeostasis (*tagE*, *tagH*, *fmt*, *ebh*, *pbp3*, *lytH*) Transcriptional regulation (*arlS*, *malR*, *kdpD*, *licR*) Translation (*prfB*, *miaA*, *leuS*, *rumA*, *rplX*, *rpmH*) Transport (*uhpT*, *oppA*, *ykoD*, *potA*, *kdpA*, *kdpB*, *corA*, *nark*, *copA*, *rarD_2*) Other (*hemC*, *hssS*) Unknown (*ybaB*, *comFC*)
A	27	Adhesion (*fnbpb*, *sdrE*, *ebhA*) Metabolism (*rpoB*, *mvaK2*, *malA*, *dagK*, *argF*, *gdpP*, *dacA*, *phoA*, *carB*, *bglK*, *tagE*, *glmM*, *lqo*) Post-translational processing (*ureE*) Transcriptional regulation (*licR*, *saeR*, *rsbV*, *bglG*) Translation (*rpmH*, *rpsJ*) Transport (*gsiC*)
B	17	*fadN*, *metG*, *hisC*, *nikE*, *lysC*, *recD2*, *acsA*, *liar*, *smc*, *leuA*, *rpsJ*
C	27	*hutH*, *ggt*, *oxyR*, *tagO*, *uvrA*, *mecA*, *purS*, *carB*, *pyrF*, *lapB*, *mnmA*, *ezrA*, *mrcA*, *artQ*, *ebh*, *rplC*, *rspJ*, *sarR*, *dapF*, *gntT*, *oatA*

Definition of abbreviation: NSMs = nonsynonymous mutations.

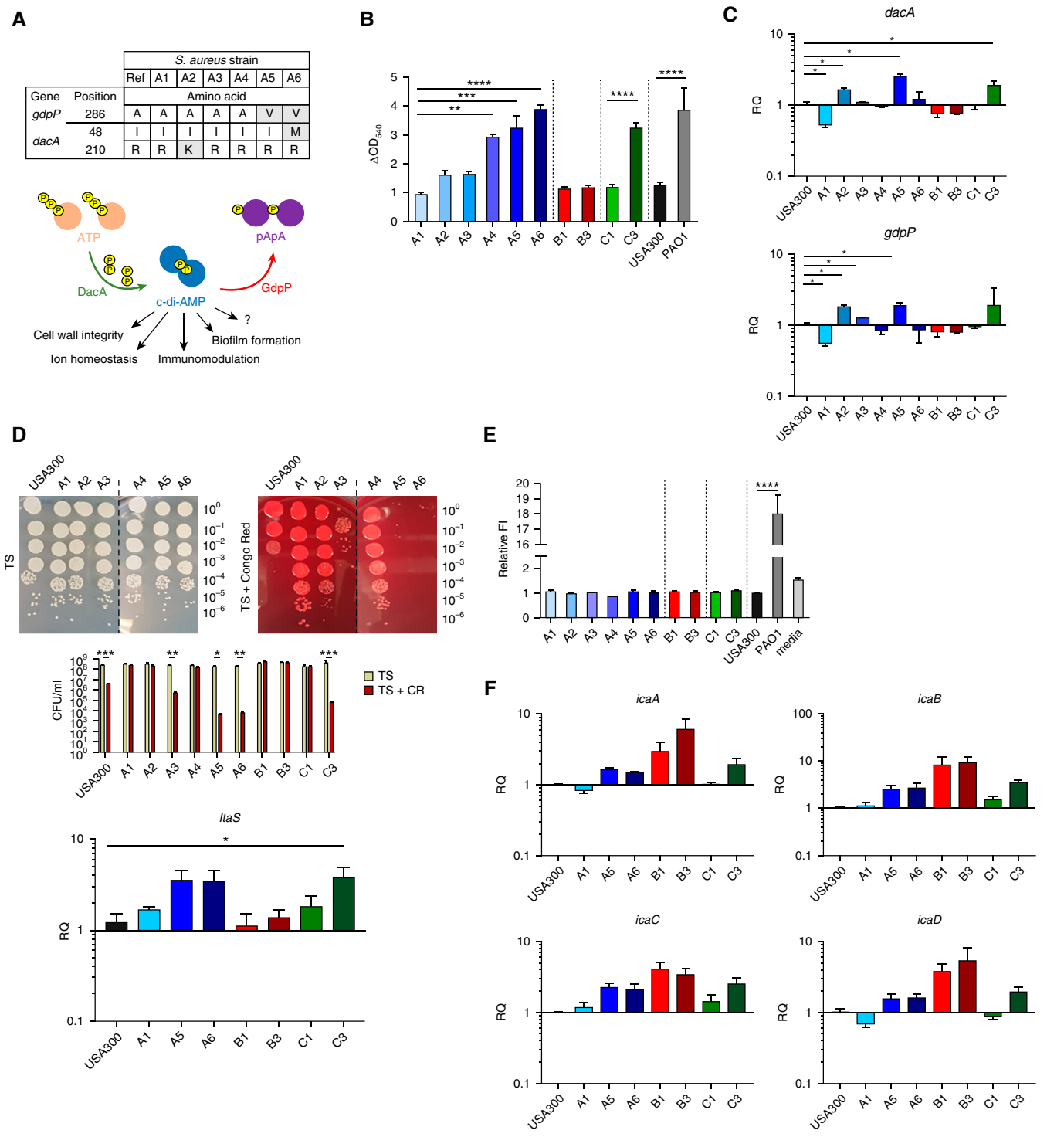

Figure 2. Biofilm-forming ability of the MRSA isolates. (*A*) Summary of NSMs observed in *gdpP* and *dacA* in MRSA isolates and schematic of the role of these genes in c-di-AMP metabolism. (*B*) Biofilm formation of the MRSA clinical isolates, MRSA strain USA300, and *Pseudomonas aeruginosa* PAO1. Data shown are from at least three independent experiments in triplicate. Statistical significance was determined by one-way ANOVA, $^{****}P < 0.0001$, $^{***}P < 0.001$, $^{**}P < 0.01$, and $^{*}P < 0.05$. (*C*) Transcription of *dacA* and *gdpP* from MRSA isolates grown in biofilm-inducing conditions. Data are shown for four biological replicates. Statistical significance was determined by Mann-Whitney *t* test, $^{*}P < 0.05$. (*D*) Effect of Congo Red (CR) on the growth of the MRSA isolates. The transcription of *ltaS*, which controls the synthesis of the cell wall component leipoteichoic acid, is also shown. (*E*) Quantification of extracellular DNA from the MRSA isolates. Data represent two independent experiments performed in triplicate. Statistical significance was determined by one-way ANOVA, $^{****}P < 0.0001$, $^{***}P < 0.001$, $^{**}P < 0.01$, and $^{*}P < 0.05$. (*F*) Transcription of the intercellular adhesion locus (*icaA/B/C/D*) from the clinical MRSA strains. For *C*, *D*, and *F*, RQ = relative quantification to wild-type (WT) LAC; TS = tryptic soy.

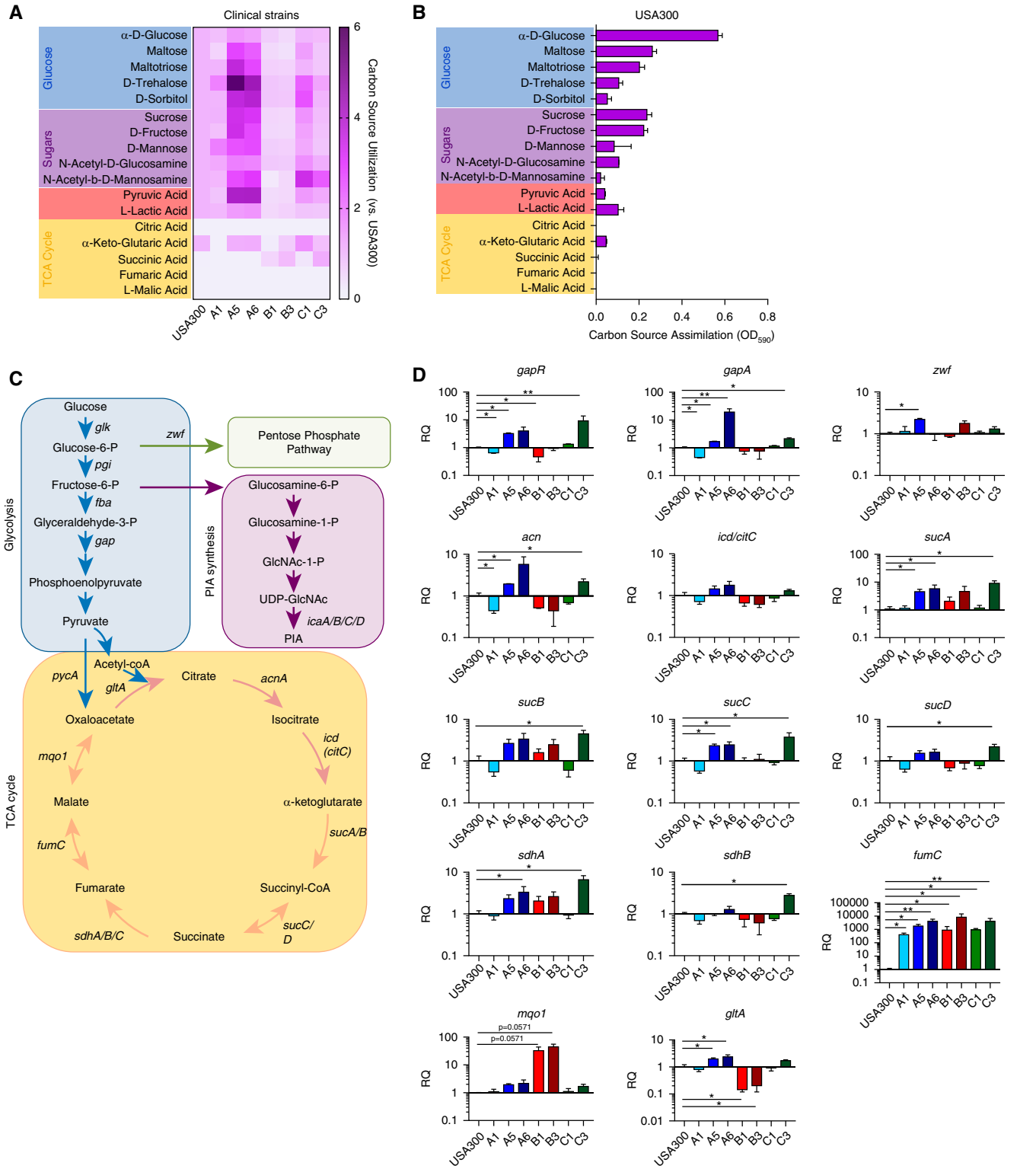

Figure 3. Metabolic adaptation of the host-adapted MRSA isolates. (*A* and *B*) Carbon source assimilation of the clinical strains relative to USA300 (*A*) and USA300 alone (*B*). The heatmap color intensity corresponds to the absorbance (OD_{590}) of the indicated strain in the presence of the indicated carbon source, normalized to the absorbance (OD_{590}) of USA300 in the same carbon source. Data represent three independent experiments. (*C*) Schematic diagram showing the major metabolic pathways in *S. aureus* and the production of polysaccharide intercellular adhesin (PIA). (*D*) Transcription of bacterial genes involved in glycolysis, the pentose phosphate pathway, and the tricarboxylic acid (TCA) cycle. Data shown are from four biological replicates. Statistical significance was determined by Mann-Whitney *t* test, $^{*}P < 0.05$ and $^{**}P < 0.01$.

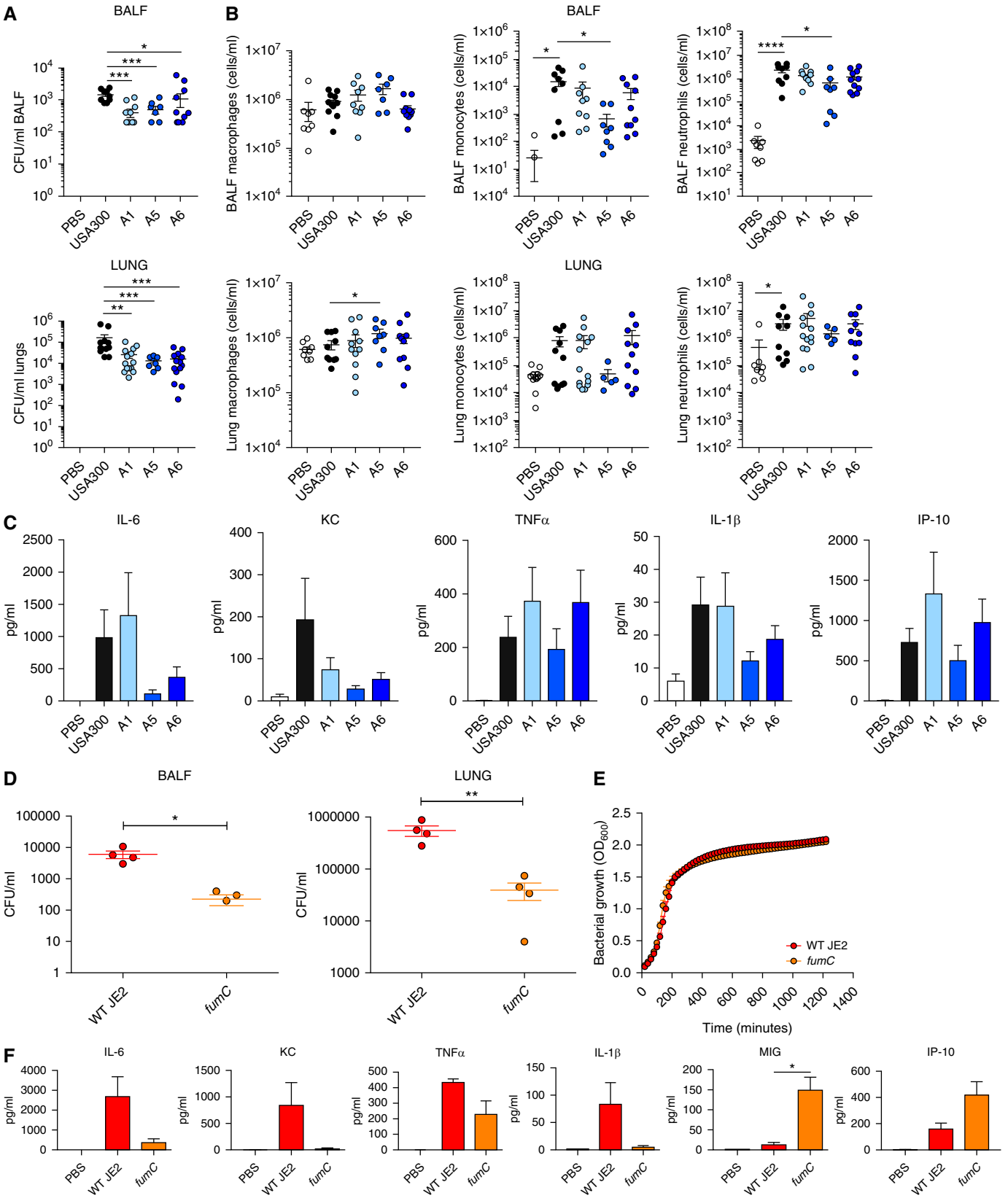

Figure 4. Role of *fumC* in *S. aureus* pathogenesis *in vivo*. (*A*) Bacterial enumeration from the BAL fluid (BALF) and lungs of mice infected with WT USA300 or the MRSA isolates A1, A5, and A6. Data are from three independent experiments done at least in triplicate. (*B*) Immune cell recruitment in the lungs of

acetyl-β-(1-6)-glucosamine (23, 24). The *ica* genes were not sites of mutation, and their expression varied among the clinical strains (Figure 2F).

Host-adapted MRSA Strains Exhibit Altered Carbon Metabolism

We further explored how the metabolic activity of the clinical isolates differed from that of the USA300 MRSA control by quantifying the assimilation of single carbon sources by each strain (Figure 3A). None of the MRSA strains consumed the tricarboxylic acid (TCA) cycle substrates citrate, fumarate, and malate. However, the host-adapted strains showed increased avidity for the glucose polymers trehalose, maltose, and sorbitol (A and C series), as well as pyruvate (A strains). The A and C series showed several similarities in preferred substrate assimilation, differing from the B series and the USA300 control, which had a marked preference for glucose use above all of the substrates offered (Figure 3B). The increased consumption of pyruvate by the A- and C-series strains and the minimal consumption of TCA cycle intermediates suggest shunting of substrates away from the TCA cycle, which generates prooxidant NADH. Instead, increased consumption of pyruvate and glucose polymers would fuel glycolysis to generate N-acetyl-glucosamine for biofilm production, which is inherently antioxidant (5).

To further determine differences in carbon source use, we monitored the expression of representative genes that are important for TCA cycle activity and gluconeogenesis by qRT-PCR (Figures 3C and 3D). Relative to the USA300 control strain, expression of *gapR*, which encodes a central glycolytic regulator (25), was increased in both the A and C series of isolates (Figure 3D). Expression of *zwf*, which is involved in the pentose phosphate pathway, was also increased in the later isolate A5. Transcription of selected TCA cycle genes was significantly altered in host-adapted MRSA strains, with a trend toward upregulation of TCA cycle enzymes as compared with USA300. This is consistent with reports that have linked *sdh* upregulation with biofilm production (26). B-series isolates showed a different pattern of TCA cycle enzyme use, with increased expression of *mqo1*, which encodes a malate:quinone oxidoreductase converting malate to oxaloacetate, yet decreased expression of *gltA*. Most impressively, in all three lineages of host-adapted strains, we observed up to 10,000-fold increases in the expression of *fumC*, which codes for the enzyme fumarate hydratase (Figure 3D), suggesting that the metabolism of fumarate and/or malate is a critical component of staphylococcal adaptation.

Participation of *fumC* Expression in the Pathogenesis of Pneumonia

Focusing on the A series of strains, which included simultaneous sputum (A5) and blood isolates (A6), we monitored MRSA clearance and the nature of the immune response elicited in a murine model of acute pneumonia, as compared with the USA300 control (Figure 4A). There was a statistically significant, but perhaps biologically less meaningful, decrease in bacterial recovery of the A-series strains from BALF and lung relative to USA300, although without discernible differences among the A-series strains themselves. The nature of the immune responses elicited was comparable for all of the MRSA strains (Figures 4B and 4C). Thus, despite the significant differences in *fumC* expression noted earlier (Figure 3D), USA300 and the A-series strains behaved comparably in an acute infection model. To appreciate how *fumC* might contribute to pathogenesis *in vivo*, we compared the clearance (Figure 4D) and immune responses (Figure 4E) associated with acute infection using a MRSA strain and *fumC* transposon mutant. Notably, there was a 2- to 3-log decrease in retention of *fumC* bacteria in murine BALF and lung, despite equivalent growth rates of WT and *fumC* bacteria *in vitro* (Figure 4E). The lower organism burden in *fumC*-infected mice was associated with a trend toward decreased induction of proinflammatory cytokines (TNF, IL-6, keratinocyte chemoattractant, and IL-1β), which supports a role for *fumC* in pulmonary infection.

Fumarate Promotes Biofilm Formation

As the murine model of acute infection does not test the significance of increased *fumC* expression over the course of chronic infection, *in vitro* studies to assess the significance of sustained *fumC* expression on MRSA were performed. FumC can reversibly hydrate fumarate or dehydrate malate, neither of which is significantly assimilated by MRSA (Figure 3A). Increasing concentrations of fumarate were tolerated up to a concentration of 500 mM, with 62.5 mM of fumarate increasing the growth of all MRSA strains tested (Figure 5A). Of note, for strains A5 and A6, these concentrations of fumarate significantly increased the formation of biofilm (Figure 5A), an effect that was not observed with the A1 strain or the WT USA300 or JE2 controls. The addition of equivalent concentrations of malate was toxic, suppressing both planktonic growth and biofilm formation (Figure 5B). This indicates that in this context, FumC functions primarily as a malate dehydratase, causing accumulation of fumarate, which is not only tolerated by the organisms but also contributes to biofilm formation in some strains. Toxicities to citrate and succinate, which suppressed growth and biofilm production, especially in the later isolates, were also observed after exposure of the MRSA strains (Figures 5C and 5D). These findings are consistent with the selective use of the TCA cycle by MRSA as an important metabolic adaptation to growth in the airways, which likely enhances persistent infection by limiting the generation of oxidants and promoting biofilm production.

Discussion

This analysis of CF-adapted MRSA isolates highlights notable differences in the metabolism of clinical strains compared with the standard USA300 LAC control, a prototype for community-acquired MRSA infection. Strain-dependent mutations were noted in each of the lineages, with evidence of ongoing diversification and adaptation.

Figure 4. (Continued). infected mice. Data shown are from at least two independent experiments. (*C*) Cytokine analysis of the BALF from infected mice. (*D*) Bacterial enumeration in the BALF and lungs of mice infected with WT JE2 or the *fumC* mutant. (*E*) Growth of WT and the *fumC* mutant in Luria-Bertani medium. Data from three independent experiments done in triplicate. (*F*) Cytokine analysis from the BALF of infected mice, $n \geq 4$ for each infected group. Statistical significance was determined by one-way ANOVA; $^{****}P < 0.0001$, $^{***}P < 0.001$, $^{**}P < 0.01$, and $^{*}P < 0.05$.

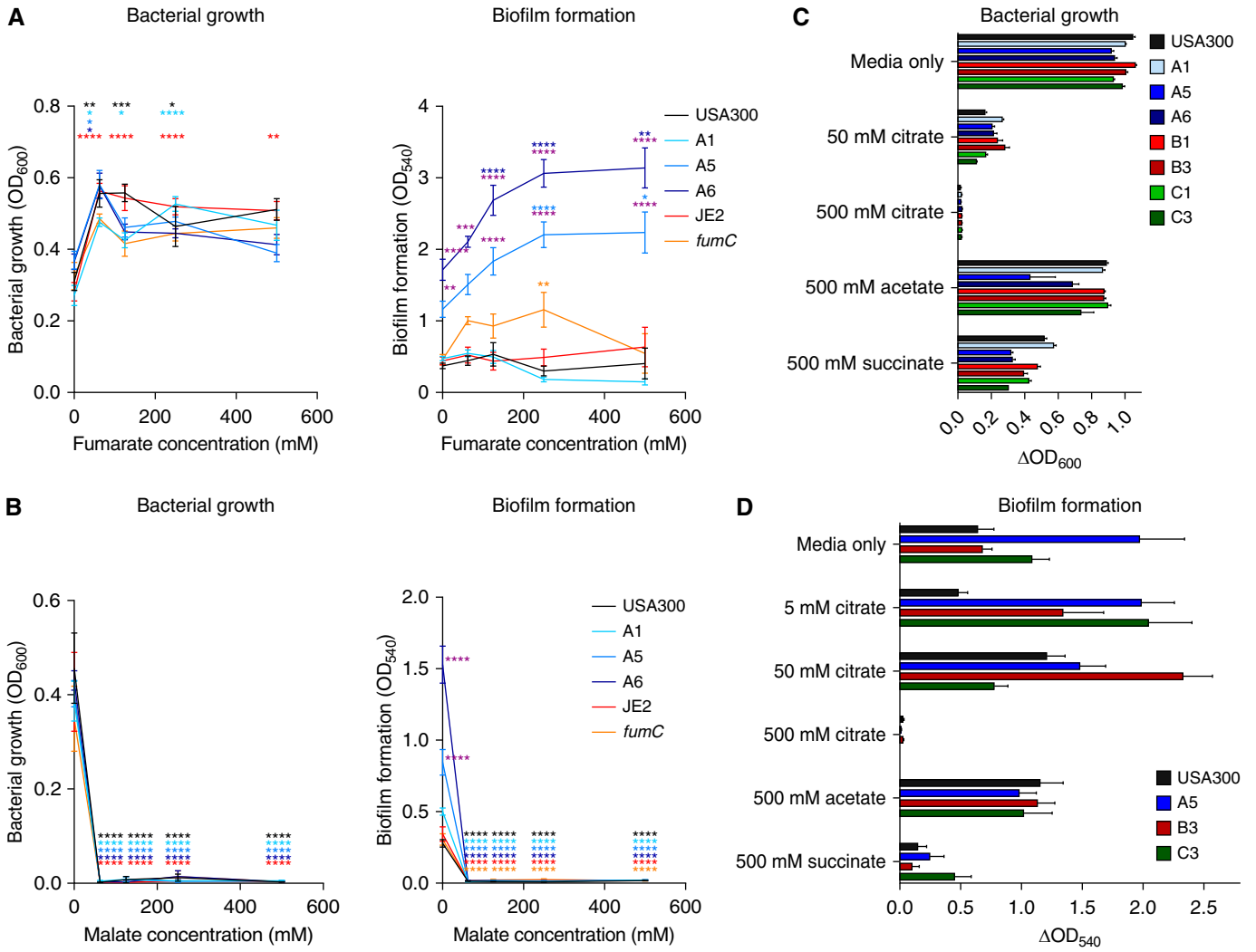

Figure 5. Fumarate enhances biofilm formation. (*A* and *B*) Bacterial growth and biofilm formation of CF host-adapted strains (WT USA300, WT JE2, and *fumC* mutant) in the presence of increasing concentrations of (*A*) fumarate and (*B*) malate. Data represent at least three independent experiments done in triplicate. Purple asterisks denote statistical difference respective to WT USA300 at the given concentration of fumarate or malate. Colored asterisks show statistical difference within the given strain across different concentrations of fumarate or malate respective to the untreated condition. Statistical significance was determined by one-way ANOVA; $^{****}P < 0.0001$, $^{***}P < 0.001$, $^{**}P < 0.01$, and $^{*}P < 0.05$. (*C*) Growth and (*D*) biofilm-forming ability as determined by crystal violet staining of MRSA strains in the presence of various concentrations of the TCA intermediates citrate, acetate, and succinate, as assessed in three independent experiments.

There were differences in gene expression in the CF isolates over time, but no definitive changes were associated with acute exacerbation. Among the genomic and transcriptional changes we documented were mutations and altered expression of *dacA* and *gdpP*, which affect turnover of the global regulator c-di-AMP. We note that these differences correlated with increased biofilm formation in some, but not all, of the host-adapted strains. In light of the recent documentation of increased expression of *dacA* and its link to biofilm formation (27), our findings confirm the clinical relevance of c-di-AMP regulation in the setting of bacterial adaptation to the CF host. Biofilm not only protects the bacteria from oxidant stress but also impedes phagocytic clearance, factors that promote the selection of these organisms from the infecting population (28, 29). In addition to its role in directing biofilm production, c-di-AMP is also involved in the induction of type I IFN signaling (27, 30, 31). IFN-β was one of the few cytokines that increased over the course of infection in the A-series isolates, consistent with the pathogenicity attributed to *S. aureus* activation of IFN-β signaling (32).

In contrast to studies of *S. aureus* strains associated with acute pneumonia in other patient populations (33), we did not observe consistent mutations in the *agr* locus, which regulates the expression of many virulence factors in the host-adapted CF isolates (34). Although we used numerous assay systems with both *in vitro* and *in vivo* outcome measurements, we were unable to identify a virulence phenotype associated with the CF strains that was significantly different from the USA300 control, beyond a 0.5-log decrease in acute infectivity. Many of the changes in gene expression that we observed were at

the level of transcription and could be readily reversed depending on environmental conditions.

Our transcriptional and metabolic studies provided more definitive evidence of MRSA adaptive changes that were not reflected in the genomic analysis. In contrast to USA300, the host-adapted MRSA strains preferentially consumed glucose polymers and selectively upregulated the portion of the TCA cycle that regulates the abundance of malate and fumarate. As the *ica* locus itself was not consistently upregulated in all of the strains, it appears that the production of biofilm is a consequence of the selective use of pathways involved in the generation of the antiinflammatory electron acceptor NADPH (5) and production of extracellular polysaccharides. Several different components of the TCA cycle were upregulated in the clinical strains, indicating the plasticity of staphylococcal metabolism and its ability to use several different metabolic mechanisms for protection from toxic oxidants. This is illustrated by the different pattern of metabolic activity observed in the B isolates as compared with the A and C isolates, which included increased *ica* gene expression in addition to elevated *fumC* expression. Most striking of all the adaptive changes we observed was the uniform upregulation of *fumC* in all three lineages of strains from the respiratory tract of patients with CF. Staphylococcal production of fumarate appears to be important for bacterial persistence within the CF lung. This may be due to fumarate's ability to act as a terminal electron acceptor in a setting of low oxygenation, which is often present within a biofilm (35–37), as well as its observed effects in promoting biofilm production and growth.

The unique airway environment in CF drives extensive bacterial metabolic reprogramming to generate ATP for ongoing metabolic needs, biofilm production, and immunoevasion (38). These selective processes generate a diverse bacterial community that is protected from the penetration of complement, antibody, and phagocytes, and thus is able to sustain chronic infection. Our analysis of the properties of CF host-adapted MRSA suggests a role for exogenous carbon substrates in therapy for MRSA pulmonary infection, as has been suggested to potentiate the activity of aminoglycosides (39). In the absence of a murine model of chronic *S. aureus* pneumonia, our *in vitro* and acute infection models indicate that host-adapted strains become increasingly susceptible to oxidants generated by the TCA cycle. Accordingly, the use of cell-permeable carboxylates as adjunctive therapy for infection in CF warrants further investigation. ■

Author disclosures are available with the text of this article at www.atsjournals.org.

References

1. Dasenbrook EC, Merlo CA, Diener-West M, Lechtzin N, Boyle MP. Persistent methicillin-resistant *Staphylococcus aureus* and rate of FEV1 decline in cystic fibrosis. *Am J Respir Crit Care Med* 2008;178:814–821.
2. Junge S, Görlich D, den Reijer M, Wiedemann B, Tümmler B, Ellemunter H, *et al*. Factors associated with worse lung function in cystic fibrosis patients with persistent *Staphylococcus aureus*. *PLoS One* 2016;11: e0166220.
3. Dasenbrook EC, Checkley W, Merlo CA, Konstan MW, Lechtzin N, Boyle MP. Association between respiratory tract methicillin-resistant *Staphylococcus aureus* and survival in cystic fibrosis. *JAMA* 2010; 303:2386–2392.
4. O'Neill LA, Pearce EJ. Immunometabolism governs dendritic cell and macrophage function. *J Exp Med* 2016;213:15–23.
5. Lemire J, Alhasawi A, Appanna VP, Tharmalingam S, Appanna VD. Metabolic defence against oxidative stress: the road less travelled so far. *J Appl Microbiol* 2017;123:798–809.
6. Gaupp R, Schlag S, Liebeke M, Lalk M, Gotz F. Advantage of upregulation of succinate dehydrogenase in *Staphylococcus aureus* biofilms. *J Bacteriol* 2010;192:2385–2394.
7. Tong SY, Davis JS, Eichenberger E, Holland TL, Fowler VG, Jr. *Staphylococcus aureus* infections: epidemiology, pathophysiology, clinical manifestations, and management. *Clin Microbiol Rev* 2015;28: 603–661.
8. Inoshima I, Inoshima N, Wilke GA, Powers ME, Frank KM, Wang Y, *et al*. A *Staphylococcus aureus* pore-forming toxin subverts the activity of ADAM10 to cause lethal infection in mice. *Nat Med* 2011;17:1310–1314.
9. Benoit JB, Frank DN, Bessesen MT. Genomic evolution of *Staphylococcus aureus* isolates colonizing the nares and progressing to bacteremia. *PLoS One* 2018;13:e0195860.
10. Windmüller N, Witten A, Block D, Bunk B, Spröer C, Kahl BC, *et al*. Transcriptional adaptations during long-term persistence of *Staphylococcus aureus* in the airways of a cystic fibrosis patient. *Int J Med Microbiol* 2015;305:38–46.
11. Treffon J, Block D, Moche M, Reiss S, Fuchs S, Engelmann S, *et al*. Adaptation of *Staphylococcus aureus* to airway environments in patients with cystic fibrosis by upregulation of superoxide dismutase M and iron-scavenging proteins. *J Infect Dis* 2018;217:1453–1461.
12. Gabryszewski SJ, Wong Fok Lung T, Annavajhala MK, Tomlinson KL, Riquelme SA, Khan IN, *et al*. Genotypic evolution of methicillin-resistant *Staphylococcus aureus* in cystic fibrosis. Presented at the North American Cystic Fibrosis Conference. October 18, 2018, Denver, CO. Abstract 337.
13. Fey PD, Endres JL, Yajjala VK, Widhelm TJ, Boissy RJ, Bose JL, *et al*. A genetic resource for rapid and comprehensive phenotype screening of nonessential *Staphylococcus aureus* genes. *MBio* 2013;4: e00537–e12.
14. Inouye M, Dashnow H, Raven LA, Schultz MB, Pope BJ, Tomita T, *et al*. SRST2: rapid genomic surveillance for public health and hospital microbiology labs. *Genome Med* 2014;6:90.
15. Seemann T. Prokka: rapid prokaryotic genome annotation. *Bioinformatics* 2014;30:2068–2069.
16. Bertelli C, Laird MR, Williams KP, Lau BY, Hoad G, Winsor GL, *et al*.; Simon Fraser University Research Computing Group. IslandViewer 4: expanded prediction of genomic islands for larger-scale datasets. *Nucleic Acids Res* 2017;45:W30–W35.
17. Arndt D, Grant JR, Marcu A, Sajed T, Pon A, Liang Y, *et al*. PHASTER: a better, faster version of the PHAST phage search tool. *Nucleic Acids Res* 2016;44:W16–W21.
18. Letunic I, Bork P. Interactive tree of life (iTOL) v3: an online tool for the display and annotation of phylogenetic and other trees. *Nucleic Acids Res* 2016;44:W242–W245.
19. Mashruwala AA, Gries CM, Scherr TD, Kielian T, Boyd JM. SaeRS is responsive to cellular respiratory status and regulates fermentative biofilm formation in *Staphylococcus aureus*. *Infect Immun* 2017;85: pii:e00157-17.
20. Vickery CR, Wood BM, Morris HG, Losick R, Walker S. Reconstitution of *Staphylococcus aureus* lipoteichoic acid synthase activity identifies Congo red as a selective inhibitor. *J Am Chem Soc* 2018; 140:876–879.
21. Wörmann ME, Reichmann NT, Malone CL, Horswill AR, Gründling A. Proteolytic cleavage inactivates the *Staphylococcus aureus* lipoteichoic acid synthase. *J Bacteriol* 2011;193:5279–5291.
22. DeFrancesco AS, Masloboeva N, Syed AK, DeLoughery A, Bradshaw N, Li GW, *et al*. Genome-wide screen for genes involved in eDNA release during biofilm formation by *Staphylococcus aureus*. *Proc Natl Acad Sci USA* 2017;114:E5969–E5978.

23. Arciola CR, Campoccia D, Ravaioli S, Montanaro L. Polysaccharide intercellular adhesin in biofilm: structural and regulatory aspects. *Front Cell Infect Microbiol* 2015;5:7.
24. Cramton SE, Gerke C, Schnell NF, Nichols WW, Götz F. The *intercellular adhesion* (*ica*) locus is present in *Staphylococcus aureus* and is required for biofilm formation. *Infect Immun* 1999;67:5427–5433.
25. Purves J, Cockayne A, Moody PC, Morrissey JA. Comparison of the regulation, metabolic functions, and roles in virulence of the glyceraldehyde-3-phosphate dehydrogenase homologues *gapA* and *gapB* in *Staphylococcus aureus*. *Infect Immun* 2010;78: 5223–5232.
26. Gaupp R, Schlag S, Liebeke M, Lalk M, Götz F. Advantage of upregulation of succinate dehydrogenase in *Staphylococcus aureus* biofilms. *J Bacteriol* 2010;192:2385–2394.
27. Gries CM, Bruger EL, Moormeier DE, Scherr TD, Waters CM, Kielian T. Cyclic di-AMP released from *Staphylococcus aureus* biofilm induces a macrophage type I interferon response. *Infect Immun* 2016;84: 3564–3574.
28. Domenech M, Ramos-Sevillano E, García E, Moscoso M, Yuste J. Biofilm formation avoids complement immunity and phagocytosis of *Streptococcus pneumoniae*. *Infect Immun* 2013;81:2606–2615.
29. Thurlow LR, Hanke ML, Fritz T, Angle A, Aldrich A, Williams SH, *et al*. *Staphylococcus aureus* biofilms prevent macrophage phagocytosis and attenuate inflammation *in vivo*. *J Immunol* 2011;186:6585–6596.
30. Commichau FM, Dickmanns A, Gundlach J, Ficner R, Stülke J. A jack of all trades: the multiple roles of the unique essential second messenger cyclic di-AMP. *Mol Microbiol* 2015;97:189–204.
31. Devaux L, Kaminski PA, Trieu-Cuot P, Firon A. Cyclic di-AMP in host-pathogen interactions. *Curr Opin Microbiol* 2018;41: 21–28.
32. Martin FJ, Gomez MI, Wetzel DM, Memmi G, O'Seaghdha M, Soong G, *et al*. *Staphylococcus aureus* activates type I IFN signaling in mice and humans through the Xr repeated sequences of protein A. *J Clin Invest* 2009;119:1931–1939.
33. Altman DR, Sullivan MJ, Chacko KI, Balasubramanian D, Pak TR, Sause WE, *et al*. Genome plasticity of *agr*-defective *Staphylococcus aureus* during clinical infection. *Infect Immun* 2018;86:pii:e00331-18.
34. Montgomery CP, Boyle-Vavra S, Daum RS. Importance of the global regulators *Agr* and *SaeRS* in the pathogenesis of CA-MRSA USA300 infection. *PLoS One* 2010;5:e15177.
35. Leys D, Tsapin AS, Nealson KH, Meyer TE, Cusanovich MA, Van Beeumen JJ. Structure and mechanism of the flavocytochrome c fumarate reductase of *Shewanella putrefaciens* MR-1. *Nat Struct Biol* 1999;6:1113–1117.
36. Uribe-Alvarez C, Chiquete-Félix N, Contreras-Zentella M, Guerrero-Castillo S, Peña A, Uribe-Carvajal S. *Staphylococcus epidermidis*: metabolic adaptation and biofilm formation in response to different oxygen concentrations. *Pathog Dis* 2016;74:ftv111.
37. Van Hellemond JJ, Tielens AG. Expression and functional properties of fumarate reductase. *Biochem J* 1994;304:321–331.
38. Foster TJ. Immune evasion by staphylococci. *Nat Rev Microbiol* 2005; 3:948–958.
39. Meylan S, Porter CBM, Yang JH, Belenky P, Gutierrez A, Lobritz MA, *et al*. Carbon sources tune antibiotic susceptibility in *Pseudomonas aeruginosa* via tricarboxylic acid cycle control. *Cell Chem Biol* 2017; 24:195–206.